Composite Structures **14** (1990) 89–111

On the Inelastic Impact of Composite Laminated Plate and Shell Structures

H. J. Lin & Y. J. Lee*

Institute of Naval Architecture, College of Engineering, National Taiwan University, 73 Chou-Shan Road, Taipei, Taiwan

ABSTRACT

The dynamic responses of composite laminated plates and shells due to inelastic impact are analyzed by using the finite element method. In the inelastic impact analysis, the structure is considered to be elastic, but the loading is idealized as inelastic. A modified isoparametric linear shell element, in which the shear deformation and rotatory inertia are taken into account, together with the theory of conservation of momentum and Newmark time integration method are used to solve the set of finite element equations. The influences of shell curvature on the impact response are investigated and discussed. The impact experiments are performed and the experimental results are in good agreement with the finite element solutions.

1 INTRODUCTION

Due to their many advantages, such as high strength, high stiffness, lightness, anti-corrosion ability, low price, workability, etc., modern composite materials are widely used in structure components. In marine engineering, for example, more and more ships of small sizes such as fishing boats, yachts, etc., use glass fiber-reinforced composite materials in ship hull construction. Because of the weak impact-resistance properties of composite materials, accidents and damage at sea have been frequently reported in recent years. Figures 1 and 2 show two typical cases of fishing boat damage due to the wave impact sustained while operating in Taiwan

*To whom correspondence should be addressed.

Composite Structures 0263-8223/90/$03·50

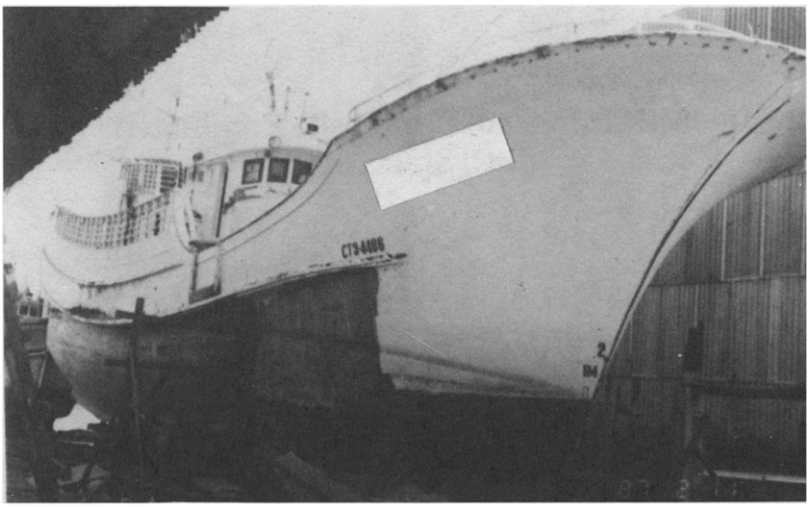

Fig. 1. Damage of a fishing boat due to wave impact—example 1.

Fig. 2. Damage of a fishing boat due to wave impact—example 2.

Channel. Thus, further understanding of impact loading, impact response and impact damage of composite material is necessary for the sake of safety.

Considerable research has been performed concerning the impact response of plates.[1–3] In practice, however, most structural components are not flat but curved in either one or two directions. It is very regrettable to find that the impact response of composite laminated shell structures have seldom been analyzed up to now. Recently, Chao *et al.*[4] used an analytical method to analyze the impact response of simply supported orthotropic cylindrical shells subjected to a given loading. Usually, the impact loading is regarded as a given function in the literature, but in the real impact situation, the impact loading is an unknown quantity to be determined. There are two ways to consider the impact loading (external force or initial condition) in the real impact in general. The first one, called elastic impact, treats the projectile and target as two elastic bodies. The impact loading is determined from the calculation of the contact law. The Hertz contact law[5] has been used by many authors. However, due to the microscopic inhomogeneous and anisotropic properties of composite laminates, the contact behavior becomes much more complicated in laminates. Thus the Hertz contact law might not be adequate in the analysis of contact formulation between the projectile and composite laminates. Tan and Sun[6] proposed an experimentally established contact law to estimate impact loading and it is evident that it is a good simulation to the real contact phenomena of a composite laminated plate. The second method, called inelastic impact, models the impact behavior of projectile and impacted node as inelastic impact with masses added together and momentum conserved, as suggested by Goldsmith.[7] Thus, after an inelastic impact, the impactor and the impacted node of target are stuck together and move with the same velocity. For simulation of slamming or some other loading having similar wavelike phenomena, the inelastic impact based on the conservation of momentum is used in this work. Experimental results show that this inelastic impact simulation is reasonable when the impactor is relatively soft and the mass of impactor is larger than the mass of the node being impacted, because under these two conditions, the impactor and the projectile will come in contact with each other smoothly. This means that for multiple impact contact, it may not be suitable to use the inelastic impact in the impact response analysis.[8] The suitability is according to the problem being analyzed.

In the present work, an eight-node isoparametric linear shell element, considering the shear deformation and rotatory inertia, is modified and used to analyze the impact response of composite laminated plates and shells under inelastic impact. The curvature effect on the impact response

of laminated cylindrical shell is investigated and discussed. The numerical results, including the deflections, stresses and strains, are presented. Experimental verification is also conducted. Impact behavior observed in the experiments is discussed and compared with the numerical results.

2 LINEAR SHELL ELEMENT FOR COMPOSITE LAMINATES

During the impact process, deformation occurs near the impact node. It is well known that shear deformation and rotatory inertia should not be ignored in impact analysis. The classical plate theory (CPT) as well as the classical shell theory (CST), however, based on the Kirchhoff hypothesis, do not consider the shear deformation and rotatory inertia. CPT and CST underestimate the deflections due to the neglect of shear deformation. When rotatory inertia is ignored, the flexural wave velocity becomes infinitely large when the wave length is infinitely small. This is physically impossible. A general curved, arbitrary shape of thin and thick shell elements proposed by Ahmad *et al.*,[9] considering the shear deformation, is modified to analyze the laminated composite plates and shells. One part of this modified shell element was discussed in Ref. 10. For the sake of completeness, its detailed formulation is described in the following.

Consider the typical eight-node isoparametric linear shell element shown in Fig. 3. (x, y, z) is the global coordinate system, (x', y', z') is the local coordinate system in which the x' and y' axes are tangent to the shell

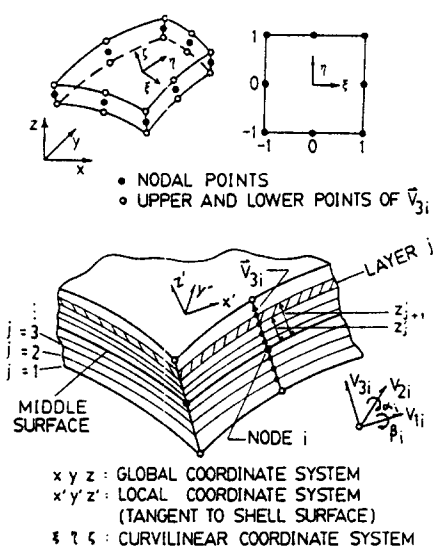

Fig. 3. The modified shell element. ●, Nodal points; ○, upper and lower points of $\mathbf{V}_{3i}$; (x, y, z), global coordinate system; (x', y', z'), local coordinate system (tangential to shell surface; (ξ, η, ζ), curvilinear coordinate system.

surface and the z' axis points in the direction of the surface normal, and (ξ, η, ζ) represents the curvilinear coordinate system which coincides with the local coordinate system. The element consists of n layers of lamina. In the thickness direction, each layer of the laminate is represented by a linear shell sub-element. The planes normal to the middle surface remain planar after the load applied is assumed to account for the shear deformation. So, the elements in various layers can be represented by the same nodes in the middle surface.

Five displacement components, u, v, w, α and β, are considered in each node. The (u, v, w) are the displacement components in the global coordinate system. (α, β) are the rotations about the y' and x' axes. In Fig. 3, the i index denotes the node number, and the j index represents the layer number $(j = 1, 2, \ldots, n)$ or sequence of interlaminae $(j = 1, 2, \ldots, n+1)$. This means that the layer between $j = 1$ and $j = 2$ is the bottom layer. The nodal points are selected in the middle surface for simplicity. It is reported[11] that because the in-plane and bending displacements are used together in the finite element variational processes, the numerical results are independent of the selection of the nodal point location.

2.1 Geometric definition of the element

Referring to Fig. 3, the geometric field of the element of a layer can be represented by the shape functions, nodal points of sub-layer and normal vector of shell surface as:

$$\begin{bmatrix} x \\ y \\ z \end{bmatrix}_j = \sum_i N_i(\xi, \eta) \begin{bmatrix} x_i \\ y_i \\ z_i \end{bmatrix}_{j(\text{mid.})} + \sum_i N_i(\xi, \eta) \frac{\zeta}{2} \mathbf{V}_{3i,j} \tag{1}$$

$$\mathbf{V}_{3i,j} = \begin{bmatrix} x_i \\ y_i \\ z_i \end{bmatrix}_{j+1} - \begin{bmatrix} x_i \\ y_i \\ z_i \end{bmatrix}_j \tag{2}$$

In eqn (1), (ξ, η) represent the coordinates tangent to the lamina plane, ζ represents the natural coordinate in the thickness direction, subscripts i and j(mid.) denote the nodal number and the coordinate field on the middle surface of jth layer lamina, respectively, and $N_i(\xi, \eta)$ are the shape functions for isoparametric element.[12] For each sub-element, $-1 \leq (\xi, \eta) \leq 1$ in the plane of the lamina, and $-1 \leq \zeta \leq 1$ between z_j' and z_{j+1}' (for isotropic materials, $|\zeta| \leq 1$ across the total thickness of the shell element).

2.2 The displacement field

The displacement field of the element of a layer can be expressed in terms of the nodal displacement and the shape functions as:

$$\begin{bmatrix} u \\ v \\ w \end{bmatrix}_j = \sum_i N_i(\xi, \eta) \begin{bmatrix} u_i \\ v_i \\ w_i \end{bmatrix} + \sum_i N_i(\xi, \eta) \left(\frac{\zeta + 1}{2} z'_{i,j+1} - \frac{\zeta - 1}{2} z'_{i,j} \right) (\mathbf{V}_{1i,j} - \mathbf{V}_{2i,j}) \begin{bmatrix} \alpha_i \\ \beta_i \end{bmatrix} \quad (3)$$

In eqn (3), (u, v, w) represent the displacements in the three principal directions of the global coordinate system and (u_i, v_i, w_i) represent the nodal displacement of node i. $\mathbf{V}_{1i,j}$ and $\mathbf{V}_{2i,j}$ are the two vectors which are normal to $\mathbf{V}_{3i,j}$, α_i and β_i are the rotations about $\mathbf{V}_{2i,j}$ and $\mathbf{V}_{1i,j}$, respectively.

2.3 The definitions of stresses and strains

The stress components, $\sigma_{x''}\sigma_{y''}\tau_{x'y''}\tau_{x'z''}\tau_{y'z'}$, and the strain components, $\varepsilon_{x''}\varepsilon_{y''}\gamma_{x'y''}\gamma_{x'z''}\gamma_{y'z'}$, defined in the local coordinate system, are considered in the formulation of the finite element equations. For simplicity, the stress components are denoted by $[\sigma]$, and the strain components are denoted by $[\varepsilon]$. The definition of the strain components are

$$[\varepsilon]^{\mathrm{T}} = [\partial u'/\partial x' \; \partial v'/\partial y' \; \partial u'/\partial y' + \partial v'/\partial x' \; \partial u'/\partial z' + \partial w'/\partial x' \; \partial v'/\partial z' + \partial w'/\partial y'] \quad (4)$$

Introducing a so-called fiber coordinate system (x'', y'', z'') aligned with the fiber direction with x'' axis, the stress–strain relationship of a lamina in terms of fiber coordinate components and local coordinate components can be expressed as:

$$\begin{aligned} [\sigma''] &= [D''][\varepsilon''] \\ [\sigma'] &= [D'][\varepsilon'] \end{aligned} \quad (5)$$

In eqn (5), the $[D'']$ and $[D']$ matrices represent the various stiffness coefficients in the fiber and local coordinate system. Since the shear moduli in the thickness direction are difficult to determine from experiments, it is assumed those values are equal to that of the in-plane shear

modulus. As in most shell analysis, the normal stress in the thickness direction is neglected in this work.

2.4 Element stiffness and mass matrix

According to the variational principle,[13] the finite element equation of motion can be derived as:

$$[M]\{d, tt\} + [K]\{d\} = \{f\} \tag{6}$$

where the $[M]$ and $[K]$ matrices represent the system mass matrix and system stiffness matrix, the $\{d\}$, $\{d, tt\}$ and $\{f\}$ vectors represent the system unknown displacement, its second-order time derivative and system loading, respectively. In the impact response analysis, since the short time interval just after impact is the key time to judge the material failure, the damping effect is therefore ignored in the formulation of the equation of motion. As mentioned before, since an element consists of n sub-elements of layers, the system matrices can be expressed as:

$$[M] = \sum_e [M]_e \quad [K] = \sum_e [K]_e \tag{7}$$

$$[M]_e = \sum_j \int [N]^{\mathrm{T}} \cdot [I] \cdot [N] \cdot \det(J) \cdot \mathrm{d}\xi \cdot \mathrm{d}\eta \tag{8}$$

$$[K]_e = \sum_j \int [B']^{\mathrm{T}} \cdot [D'] \cdot [B'] \cdot \det(J) \cdot \mathrm{d}\xi \cdot \mathrm{d}\eta \cdot \mathrm{d}\zeta \tag{9}$$

$$\mathrm{dia}([I]) = (\rho, \rho, \rho, \rho t^2/12, \rho t^2/12) \tag{10}$$

In eqns (7)–(10), the e index represents the element number, the $[N]$ matrix is the relationship between displacement field and nodal displacements of eqn (3), ρ is the mean mass density per unit area, t is the thickness of the laminate, $[B']$ represents the strain–displacement relation of eqn (4), and $\det(J)$ is the determinant of Jacobi transformation matrix.

The 3×3 Gaussian integration rule is used in the numerical integration of the mass matrix $[M]$. Although the diagonal mass matrix[14] will give more accurate value of natural frequencies than that of the lump or consistent mass matrix for a simply supported square plate, the consistent mass matrix is used in the finite element program. The reduced $2 \times 2 \times 2$ Gaussian integration rule is used in the formulation of stiffness matrix $[K]$. The Newmark time integration method with constant acceleration is used to solve the finite element equations for the reasons of simplicity and unconditional stability.

3 INELASTIC IMPACT

In order to simulate a shapeless projectile impact, such as the impact of wave or liquid, the inelastic impact is used to model the contact behavior between the projectile and the impacted node of the finite element. In the initial state, the structures are at rest and the projectile is moving with a constant velocity. As the impact occurs, the projectile hits the plate or shell and sticks on the impacted node of the finite element. The theory of conservation of momentum is assumed, which means that the total momentum is conserved before and after impact:

$$m_p V_p = (m_p + m_n) V_0 \tag{11}$$

where m_p is the mass of the projectile, m_n is the mass of the impacted node and V_p is the velocity of the projectile. Equation (11) can be rewritten as:

$$V_0 = m_p V_p / (m_p + m_n) \tag{12}$$

The calculated V_0 is used as the initial velocity of the impacted node of the finite element, and the mass of projectile, m_p, is added to the mass of the impacted node, m_n.

4 NUMERICAL RESULTS AND DISCUSSION

In the following numerical analysis, the material properties, density and dimensions used were taken from Taketa[15] and Petersen[8] for the reason of comparison. The laminating sequence of $[0_5^\circ/90_5^\circ/0_5^\circ]$ is used. The properties of Scotchply 1002 composite with epoxy matrix and E glass fiber used are given as:

$E_1 = 40{\cdot}00$ GPa $\quad E_2 = 8{\cdot}27$ GPa

$\nu_{12} = 0{\cdot}26$ $\quad G_{12} = G_{13} = G_{23} = 4{\cdot}14$ GPa

$h = 0{\cdot}003\,35$ m $\quad \rho = 1901{\cdot}5$ kg/m^3

where E_1 and E_2 represent Young's moduli in the fiber or transverse direction of the lamina, respectively, G_{ij} is shear modulus in various planes, ν_{12} is Poisson's ratio in the lamina plane, and h and ρ are the thickness and density of the laminates, respectively. The plate and shell are clamped on the edges with length a (x-axis) and width b (y-axis) both equal to 0·14 m. Cylindrical shells curved in the x direction are considered. The 0° direction is arranged along the x-axis. Two cylindrical shells with radii of 0·1 m (shell no. 1) and 0·05 m (shell no. 2) and one plate (with infinite radius) are analyzed. The impactor has a mass of 0·014 175 kg and

an initial velocity of 39·7 m/s. The impacted face of the target is called the front face (or upper surface), the other side is called the back face (or lower surface). The domain of numerical analysis of the cylindrical shell is bent back to a plane. Thus the numerical results of plate and shells have the same expressive domain with 0·14 m length and 0·14 m width. The dynamic response is expressed in the time from 10 μs to 250 μs. Because of the material and geometric symmetry, only a one-quarter region with symmetric conditions and 6×6 (36 element) mesh is analyzed. The dynamic response, including lateral deflection, normal stresses and shear stresses at the uppermost and lowest Gaussian points along the x and y axes, are expressed.

The deformed configuration of the composite laminated plate and shell are shown in Fig. 4. The magnitude of the response is magnified about 46·67 times. The numerical results of plate are in good agreement with those of Petersen,[8] although a different mass matrix is used. In Fig. 4, only a quarter region is analyzed. Using the quantities interpolation and technique of grid generation, the deformed configuration of full domain is generated. For the reason of simplicity, only the detailed results of shell no. 2 and the plate are presented. Figure 5 shows the lateral deflection (w) at the impacted node of the plate and shells. From these results, it can be seen that the amplitude of deflection and the rebound time both decrease as the curvature increases. But in the initial stage the curvature effect on the lateral displacement is very small. In fact, they are almost equal up to 60 μs. It can be explained that the inertia force is dominant in resisting the external loading in the earlier stage after impact. Therefore the contribution of structural rigidity in resisting the external load is relatively small, and causes nearly the same lateral deflection of plate and shells just after impact.

The deflection (w) along the x and y axes in the central sections from time 10 μs to 50 μs and from 50 μs to 200 μs is shown in Figs 6 and 7. In Fig. 6(a), the cylindrical shell has a smaller deflection due to the curvature effect. In the y axis, because the curvature effect increases the bending rigidity, the shell has a higher wave speed than that of the plate. For example, the distance from the impacted node to the nearest point which intersects the zero deflection line is 20 mm in the plate and 25 mm in shell no. 2 at 50 μs (Fig. 6(b)). The larger the bending rigidity, the faster the speed of the stress wave, as is observed in Fig. 6. It can be seen that the distance from the impacted node to the nearest point which intersects the zero deflection line is 30 mm along the x axis and 20 mm along the y axis of the plate. The deflection occurred near the impacted node, but remained stationary near the edges in the time just after impact occurred. As time increases, the disturbance begins to propagate to the edges, and then is

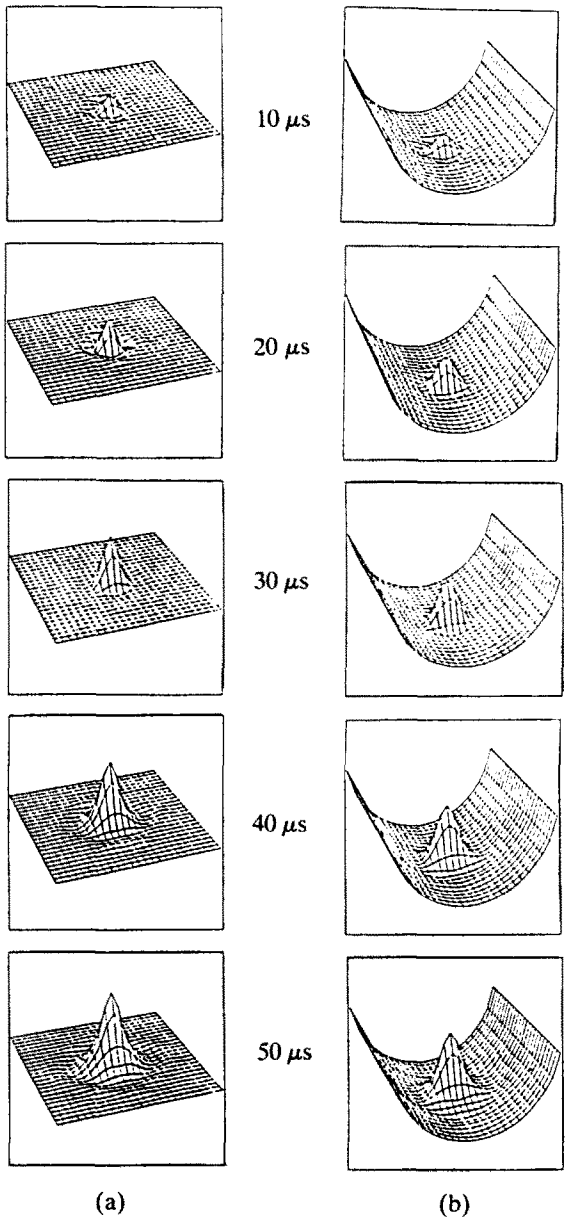

Fig. 4. The deformed configuration of laminates (a) the plate and (b) shell no. 2.

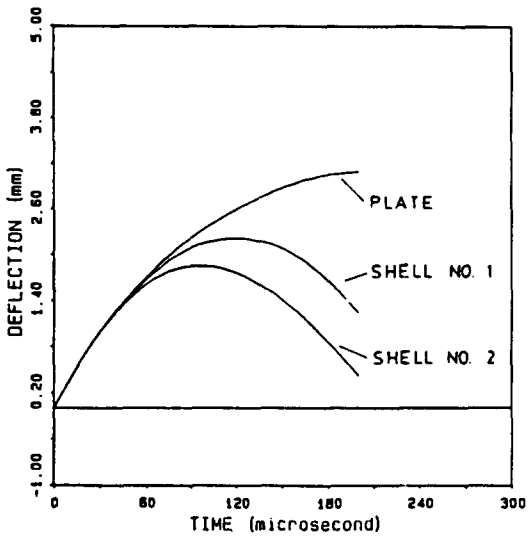

Fig. 5. Lateral deflection of impacted nodes of the plate, shell no. 1 and shell no. 2.

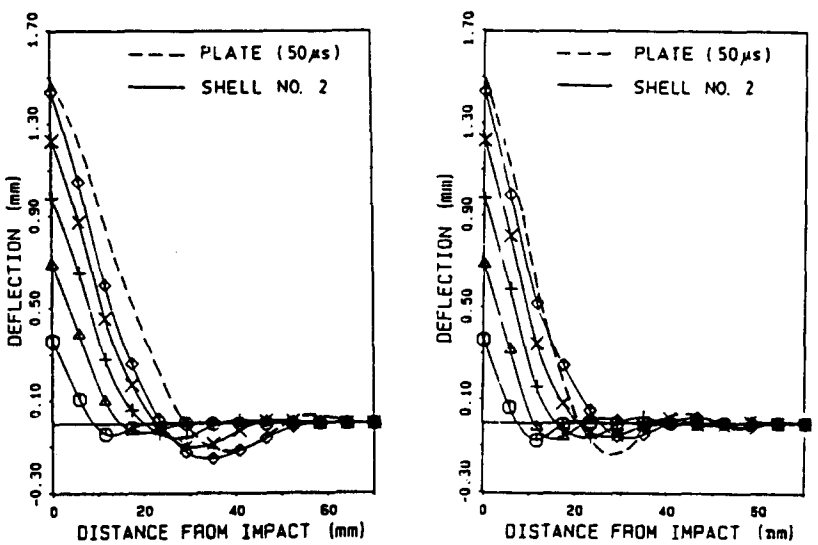

Fig. 6. The deflection of the plate (– – –) at 50 μs and shell no. 2 (——) along (a) the x axis and (b) the y axis for times from 10 μs to 50 μs. ○, 10 μs; △, 20 μs, +, 30 μs; ×, 40 μs; ◇, 50 μs.

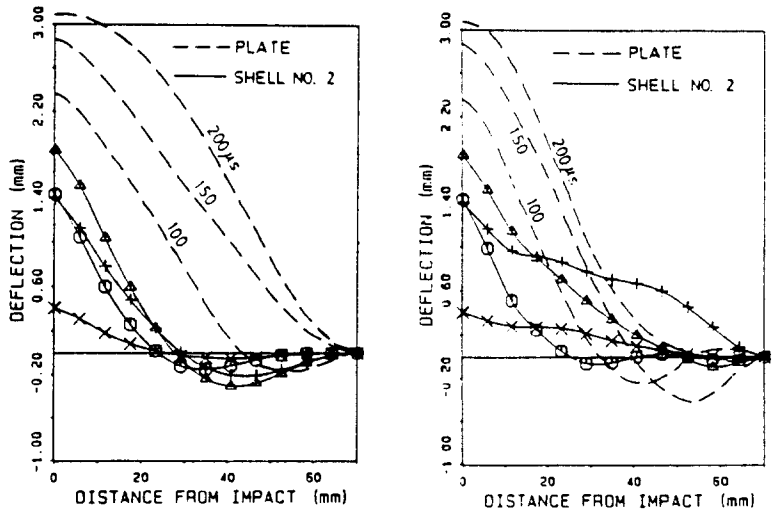

Fig. 7. The deflection of the plate (– – –) and shell no. 2 (——) along (a) the x axis and (b) the y axis for times from 50 μs to 200 μs. ○, 50 μs; △, 100 μs; +, 150 μs; ×, 200 μs.

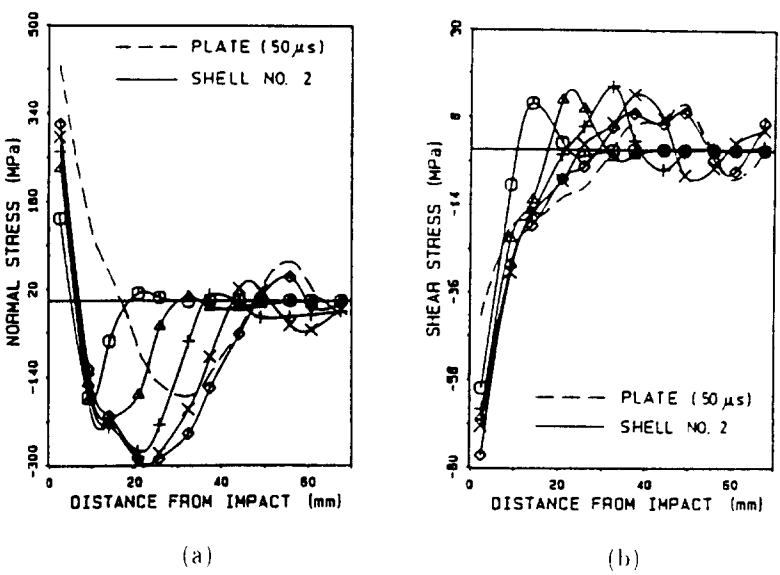

Fig. 8. The normal stress (a) and the shear stress (b) of the plate (– – –) at 50 μs and shell no. 2 (——) at the lowest Gaussian points along the x axis for times from 10 μs to 50 μs. ○, 10 μs; △, 20 μs; +, 30 μs; ×, 40 μs; ◇, 50 μs.

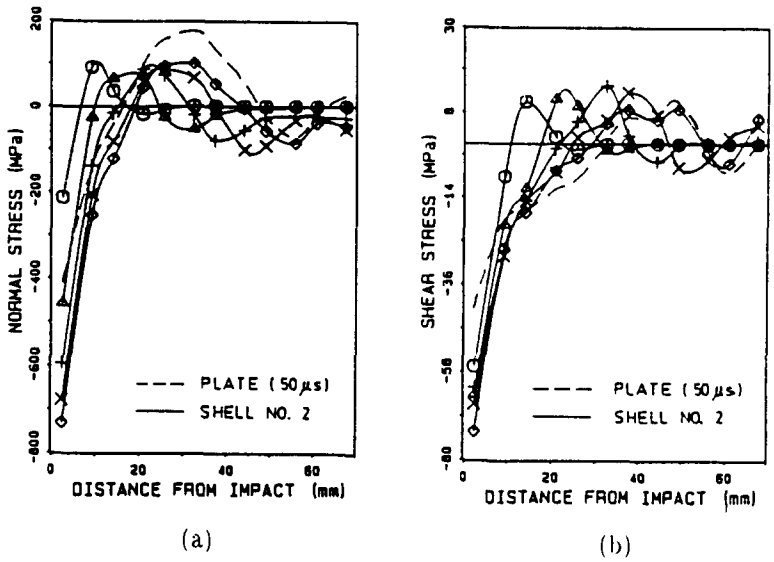

Fig. 9. The normal stress (a) and the shear stress (b) of the plate (– – –) at 50 μs and shell no. 2 (——) at the uppermost Gaussian points along the x axis for times from 10 μs to 50 μs. ○, 10 μs; △, 20 μs; +, 30 μs; ×, 40 μs; ◇, 50 μs.

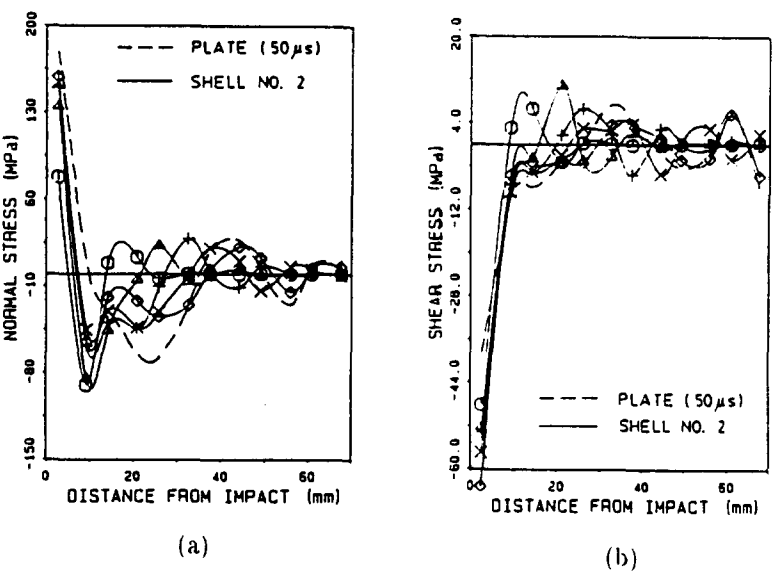

Fig. 10. The normal stress (a) and the shear stress (b) of the plate (– – –) at 50 μs and shell no. 2 (——) at the lowest Gaussian points along the y axis for times from 10 μs to 50 μs. ○, 10 μs, △, 20 μs; +, 30 μs; ×, 40 μs; ◇, 50 μs.

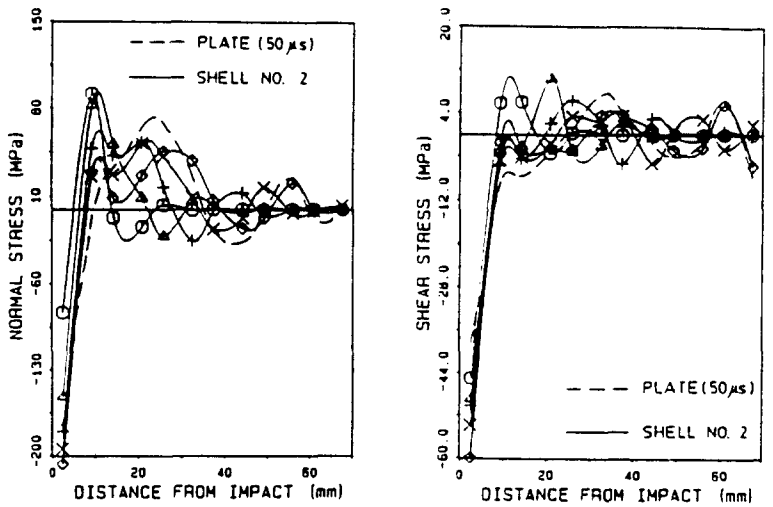

Fig. 11. The normal stress (a) and the shear stress (b) of the plate (– – –) at 50 μs and shell no. 2 (——) at the uppermost Gaussian points along the y axis for times from 10 μs to 50 μs. ○, 10 μs, △, 20 μs; +, 30 μs; ×, 40 μs; ◇, 50 μs.

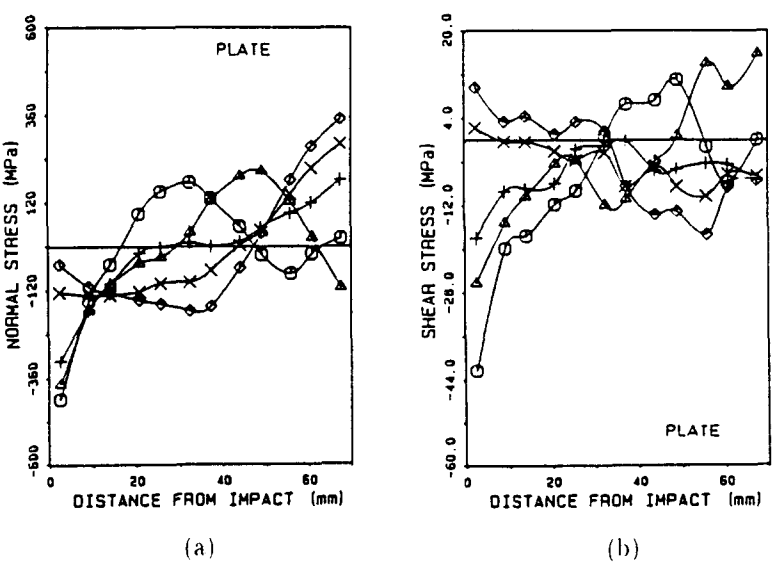

Fig. 12. The normal stress (a) and the shear stress (b) of the plate at the uppermost Gaussian points along the x axis for times from 50 μs to 250 μs. ○, 50 μs; △, 100 μs; +, 150 μs; ×, 200 μs; ◇, 250 μs.

reflected, due to the boundary. The deflection is positive near the impacted node but negative at a distance, owing to the inertia force effect.

Figures 8–11 show the normal stress ($\sigma_{x'}$ or $\sigma_{y'}$) and Figs 12–15 the average shear stress ($\tau_{x'z'}$ or $\tau_{y'z'}$) response calculated at the uppermost and lowest Gaussian points in the middle sections along the x and y axes of short time and long time, respectively. The bending stress waves are the dominant stress in the symmetric laminated plate. From Fig. 8(a) and Fig. 10(a) it can be seen that there exists an in-plane stress wave in the shells. Normal stress, of same magnitude but opposite in sign, and average shear stress, of same magnitude and sign, are found in the lower (back face) and upper (front face) surfaces of the plate. However in the case of the shells, there is more compressive normal stress in the front face and less tensile stress in the back face. Tensile stress on the lower surface and compressive stress on the upper surface in the near region of impact node is found, while in the region distant from the node it is reversed. The value of shear stress is negative in the near region of impact and positive in a distant place. Stress wave propagation from the impacted node to the near region is observed too. In Figs 12–15, the results of stress response at the uppermost Gaussian points in the long time interval are presented. It can be seen that the stress distribution is more complicated after the reflection of stress waves. Due to the reflection of stress waves, normal or shear stress may change sign after 250 μs near the impacted node of shell no. 2.

5 THE EXPERIMENTAL VERIFICATION

An elastic impact test of composite laminated plate and cylindrical shells is conducted here. The graphite/epoxy structures of one plate and two cylindrical shells with dimensions of 149 mm × 149 mm × 1·7 mm are used as the impact targets. The material constants shown in Table 1 are taken from the material testing done according to the rules of the Society of Fiber Reinforced Plastic of Japan. The laminating sequence of $[0_5^\circ/90_5^\circ/0_5^\circ]$ is applied in the case of the plate and $[90_5^\circ/0_5^\circ/90_5^\circ]$ and $[0_5^\circ/90_5^\circ/0_5^\circ]$ in the case of the shells. The 0° direction is arranged along the x axis and the radius of the cylindrical shell is 125 mm. The $[90_5^\circ/0_5^\circ/90_5^\circ]$ and $[0_5^\circ/90_5^\circ/0_5^\circ]$ cylindrical shells are named shell no. 3 and 4, respectively. Eight strain gages are placed at different locations, as shown in Fig. 16, to sense the dynamic strain histories. Strain gage nos 1–4 are placed on the back face and nos 1′–4′ are placed on the front face with reference to the impactor. An H.P. 5183U digitizing oscilloscope and two Kyowa DCV 230 v strain gage amplifiers are used to capture strain responses. The impact–force transducer of Model 200A5, marketed by PCB Piezotronics Inc., is used also to

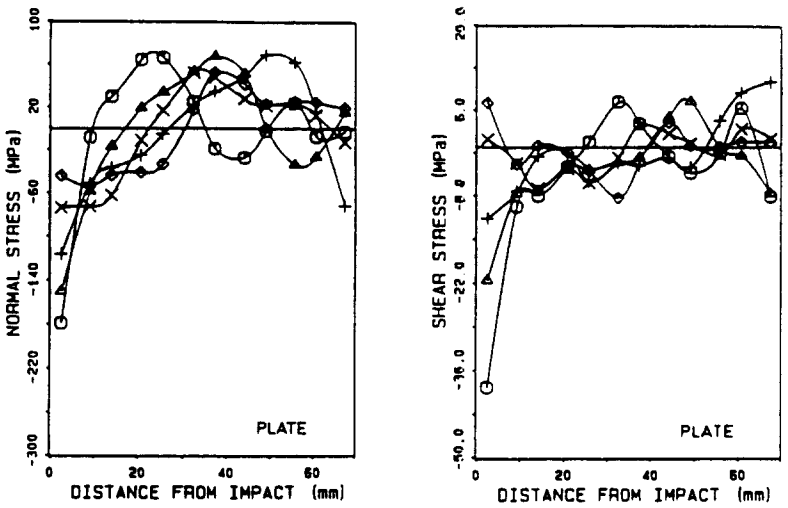

(a) (b)

Fig. 13. The normal stress (a) and the shear stress (b) of the plate at the uppermost Gaussian points along the y axis for times from 50 μs to 250 μs. ○, 50 μs; △, 100 μs; +, 150 μs; ×, 200 μs; ◇, 250 μs.

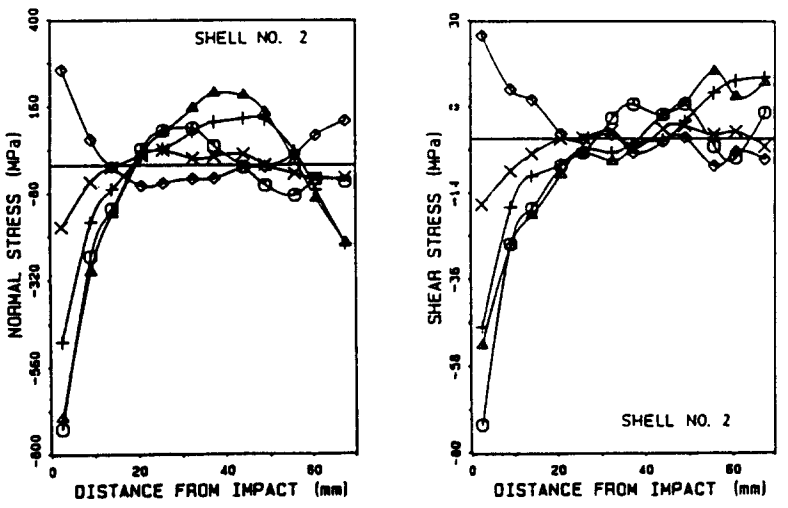

(a) (b)

Fig. 14. The normal stress (a) and the shear stress (b) of shell no. 2 at the uppermost Gaussian points along the x axis for times from 50 μs to 250 μs. ○, 50 μs; △, 100 μs; +, 150 μs; ×, 200 μs; ◇, 250 μs.

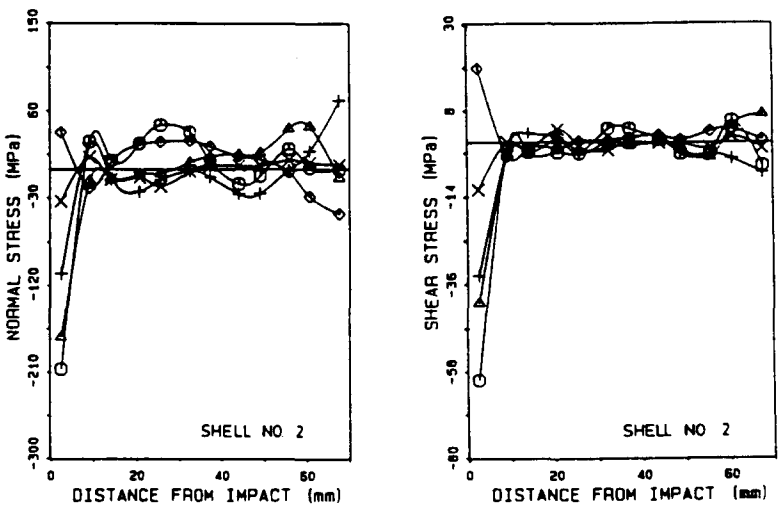

Fig. 15. The normal stress (a) and the shear stress (b) of shell no. 2 at the uppermost Gaussian points along the y axis for times from 50 μs to 250 μs. ○, 50 μs; △, 100 μs; +, 150 μs; ×, 200 μs; ◇, 250 μs.

TABLE 1
The Material Constants of the Graphite/Epoxy Laminates Used in the Experiments

Young's moduli		*Shear modulus*	*Poisson's ratio*	*Mass density*
E_1 *(GPa)*	E_2 *(GPa)*	(G_{12}) *(GPa)*	(ν_{12})	(ρ) *(kg/m × m)*
108·07	8·44	3·32	0·28	2·50

record the impact force history as a reference. The targets are hung with three strings at the center and the corners to achieve the free boundary condition. The steel impactor has a spherical nose with 12·7 mm diameter and total length of 28 mm approximate to the shape used by Tan and Sun.[6] The masses of impactor and target are 0·038 87 kg and 0·055 63 kg, respectively. Using four strings to maintain the balance of the impactor, a velocity of 1·704 m/s for the impactor is produced. Because only two strain gage amplifiers are used, the experiments are repeated many times under the same conditions in order to record the responses of various strain gages.

A quarter region of the target is modeled by 36 (6 × 6) shell elements owing to the symmetry of geometry and material, because the Newmark

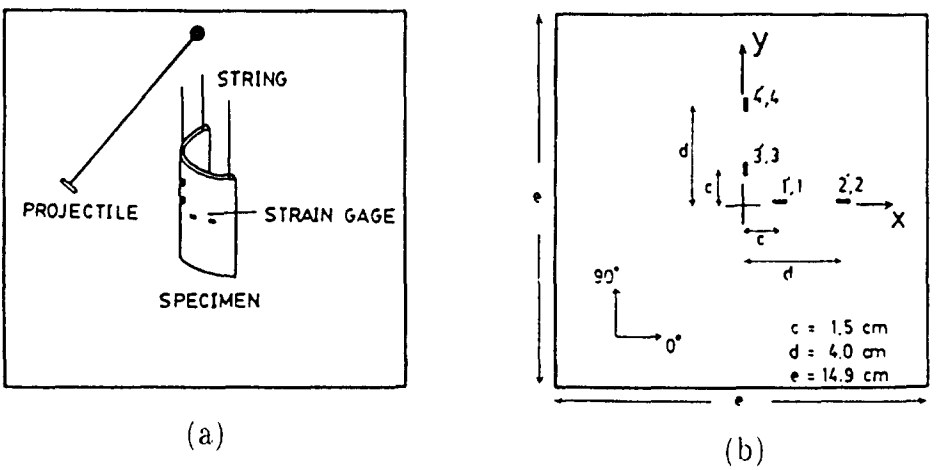

Fig. 16. Schematic diagrams for (a) the impact test and (b) strain gage locations.

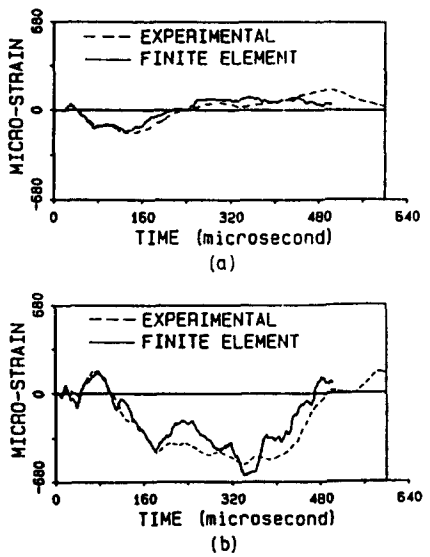

Fig. 17. Strain response histories of laminated plate. (a) Strain gage no. 2, (b) strain gage no. 4. (---) Experimental results, (——) finite element method results.

time integration method is an unconditional stable scheme. Thus according to the contact duration of plate and cylindrical shell in experiments, the Newmark time integration method with time steps of 0·5, 1·0, 2·0 μs are used. It is found that the solutions are in good agreement for various time steps. Thus the time step of 2 μs is used in the following numerical analysis.

Figures 17–20 show the strain response histories of plate and shell at the lowest or uppermost Gaussian points in the location of the strain gage. The experimental data are factored by a value of 0·859 to represent the values at Gaussian points. It can be seen that the experimental results of elastic impact fit very well with the numerical results of inelastic impact. From the results of Fig. 21, it is found that the impactor and target come into contact before 500, 700 and 1200 μs for shell no. 2, shell no. 1 and the plate, respectively. This phenomenon matches with the assumption of inelastic impact. Due to the limitation of frequency response of experimental instruments, the much more smooth records of experimental strain response are observed. It is evident that the bending wave is the dominant

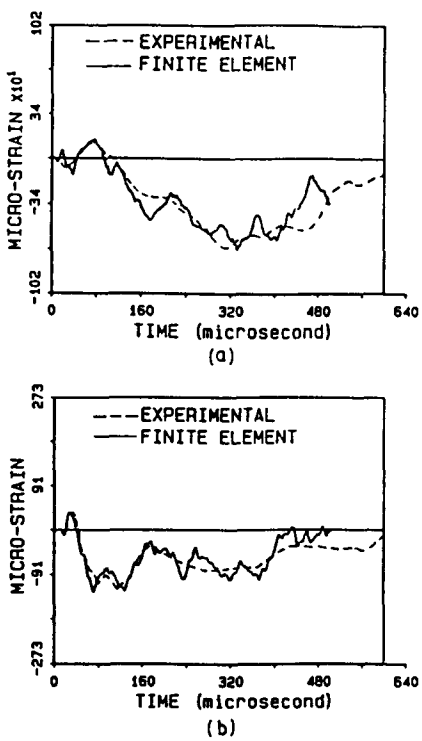

Fig. 18. Strain response histories of shell no. 3. (a) Strain gage no. 2, (b) strain gage no. 4. (– – –) Experimental results, (——) finite element method results.

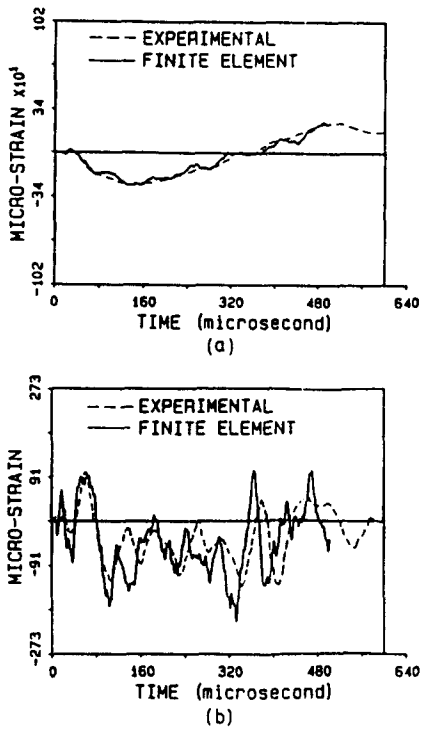

Fig. 19. Strain response histories of shell no. 4. (a) Strain gage no. 2, (b) strain gage no. 4. (---) Experimental results, (——) finite element method results.

phenomenon in the plate (Fig. 20(a)), but in the case of the shells, the in-plane stress wave exists, although the bending wave is also dominant (Fig. 20(b)). From Figs 17–19, the smaller strain response along the direction which possess larger bending rigidity, i.e. along the x axis of the plate and shell no. 4 and along the y axis of shell no. 3, is observed too. Under the given loading conditions, it is well known that the strain response in a shell structure is smaller than that in a plate. From Figs 17–19, it can be seen that the strain response of the shells is nearly the same as that of the plate generally and may be larger than that of the plate in some records. This phenomenon can be explained from Fig. 21: the more the lateral rigidity, the higher the impact load produced. In Fig. 21, the multiple contacts of shell no. 4 and different contact durations are also observed. Therefore, it may be concluded that targets with larger lateral rigidity (curvature effect) will experience a larger impact force, shorter contact duration and multiple contacts. It is evident that the finite element results agree very well with the experimental results.

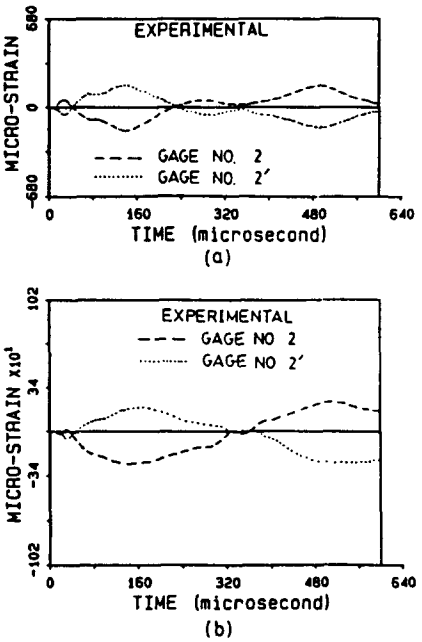

Fig. 20. Experimental strain response histories of (a) the plate and (b) shell no. 4. (– – –) Strain gage no. 2, (——) strain gage no. 4.

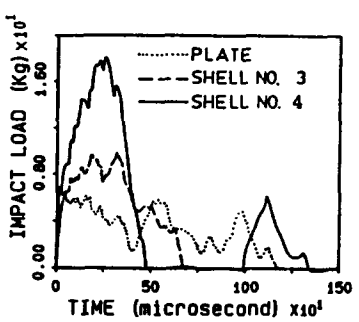

Fig. 21. Impact force histories of the plate (·····), shell no. 3 (– – –) and shell no. 4 (——).

6 CONCLUSIONS

The dynamic response of composite laminated plates and shells under inelastic impact are analyzed by using the modified linear shell element. In the inelastic impact analysis, the structure is considered to be elastic, but the loading is idealized as inelastic. Dynamic responses, including the deflection and stresses, are presented, and the effects of curvature on the

dynamic responses are compared and discussed. It is found that the existence of curvature tends to decrease the lateral deflection and the rebound time of the structures, while increasing the compressive normal stress in the front face being impacted. Also, the bending rigidity in the axial direction of cylindrical shell increases due to the curvature effect.

An impact experiment is conducted on graphite/epoxy laminated plate and shells with a free boundary condition. From the experimental results, it is concluded that the larger lateral rigidity of the target produced a larger impact force, shorter contact duration and multiple contacts. It is also demonstrated that the finite element solution matched very well with the experimental results.

ACKNOWLEDGMENT

This work was supported by the National Science Council, People's Republic of China, under the Grant No. NSC78-0405-E002-11. The authors would like to express their sincere appreciation to Dr C. T. Sun (Professor of Purdue University, USA) for his invaluable advice and continuous support.

REFERENCES

1. Sun, C. T. & Chen, J. K., On the impact of initially stressed composite laminates. *Journal of Composite Materials*, **19** (1985) 490–504.
2. Chen, J. K. & Sun, C. T., Analysis of impact response of buckled composite laminates. *Composite Structures*, **3** (1985) 97–118.
3. Caprino, G., Crivelli, I. & Dillio, A., Composite materials response under low-velocity impact. *Composite Structures*, **2** (1984) 261–71.
4. Chao, C. C., Tung, T. P. & Lee, S. C., Response of orthotropic cylindrical shells subjected to impact loading. In *International Conference on Advanced Composite Materials and Structures*, Taipei, Taiwan, May 1987, pp. 705–16.
5. Hertz, H., Über die Berührung fester elastischer Körper. *Journal of Reine Angle Math, Crelle*, **92** (1881) 155.
6. Tan, T. M. & Sun, C. T., Use of statical indentation laws in the impact analysis of laminated composite plates. *Journal of Applied Mechanics*, **52** (1985) 6–12.
7. Goldsmith, W., *Impact; the Theory and Physical Behavior of Colliding Solids*. Edward Arnold, London, 1960.
8. Petersen, B. R., Finite element analysis of composite plate impacted by a projectile. PhD dissertation, The University of Florida, USA, 1985.
9. Ahmad, S., Irons, B. M. & Zienkiewicz, O. C., Analysis of thick and thin shell structures by curved finite elements. *International Journal for Numerical Methods in Engineering*, **2** (1970) 419–51.

10. Lee, Y. J., Lin, H. J. & Lin, C. C., Buckling analysis of composite laminates. *Composite Structures*, **12** (1988), 133–48.
11. Lin, H. J. & Lee, Y. J., The stress analysis of unsymmetric composite beams, plates and shells using a modified linear shell element. In *The Twelfth National Conference on Theoretical and Applied Mechanics*, Taipei, Taiwan, December 1988, pp. 747–54.
12. Hinton, E. & Owen, D. R. J., *Finite Element Programming*. Academic Press, London, 1977.
13. Zienkiewicz, O. C., *The Finite Element Method*, 3rd edn. McGraw-Hill, 1971.
14. Hinton, E., Rock, T. & Zienkiewicz, O. C., A note on mass lumping and related processes in the finite element method. *International Journal of Earthquake Engineering and Structural Dynamics*, **4** (1976) 245–9.
15. Takeda, N., Experimental studies of the delamination mechanisms in impacted fiber-reinforced composite plates. PhD dissertation, The University of Florida, USA, 1980.